Averaging Technique for the Modeling of STATCOM and Active Filters

M. Tavakoli Bina, *Senior Member, IEEE*, and Ashoka K. S. Bhat, *Fellow, IEEE*

***Abstract*—This paper introduces average circuit models for switch mode shunt converters coupled with power systems such as active filters and static compensators (STATCOM). These devices absorb or deliver reactive power to the utility network by employing either a fixed or a variable switching frequency (e.g., pulsewidth modulation voltage control or hysteresis current control). Analysis and simulation of these exact devices could be complex under transient and steady state conditions. Ongoing investigations on design of a practical STATCOM show that performing these kind of simulations (e.g., with PSpice) are very sluggish. Here both the fixed and variable switching frequency shunt devices are modeled using an averaging approach, by deriving their state-space equations. An average operator is defined, and applied to the state equation to get averaged mathematical models. Expansion of these models will eventually lead us to average circuit models. Further, the ripple is approximated to provide a correction to the average model. The resulting models produce much faster simulations than their exact devices. Theoretical considerations show that the averaged models agree well with the original system, and this is confirmed by PSPICE and MATLAB simulations. Additionally, experimental results are presented to validate the developed models.**

***Index Terms*—Active filter (AF), average circuit model, averaging technique, static compensators (STATCOM), state-space averaging.**

I. Introduction

THE use of FACTS controllers can potentially overcome some problems of electromechanically controlled transmission systems. An active filter (AF) can be employed as a parallel device in ac power distribution systems to provide the load harmonic currents [1]. Also, a static compensator (STATCOM) is used in both transmission and distribution systems to control reactive power, unwanted harmonics, and three-phase voltage unbalance [2], [3]. Different voltage-sourced inverter topologies could be implemented using gate turn-off thyristors (GTOs) and/or insulated gate bipolar transistors (IGBTs) for these high power utility applications.

The analysis of a power electronic system is complex, due to its switching behavior. Therefore, there is a need for simpler, approximate models. One common approach to the modeling of power converters is averaging. This approximates the operation of the discontinuous system by a continuous-time model. This model produces waveforms that approximate the time-averaged waveforms of the original system, while simplifying analysis and making it easier to understand the system's behavior under steady state and transient conditions. Averaged models have the advantage that they speed up simulation. They can also be used for control and design purposes, in power systems issues such as voltage and current unbalance investigations.

This paper introduces average models for STATCOM and AF, which are used to predict the performance of complete working devices much faster than their exact models at the expense of losing some of the high frequency details in the waveforms. Although an average model was proposed and used in the analysis of converters [4], their use in STATCOM and AF is not reported in the literature. Note that here the modeling needs to be concerned with the main power system frequency of 50/60 HZ in addition to the dc voltages of the converter. Also, when the modulation strategy employs variable switching frequency, then it is necessary to decide on a convergent averaging period for the model. In fact, possible switching status within an averaging period can be different for fixed and variable frequency modulation. Thus, fixed and variable switching frequencies are analyzed separately. We start with the time-varying state-space equations of AF and STATCOM, approximating them by averaged equations to obtain a mathematical model. Then an equivalent circuit model is introduced, which provides a useful tool for analytical purposes. Finally, we extend our approximate model to incorporate ripple effects. The average model gives good agreement with the original system, as demonstrated using PSpice and MATLAB simulations along with practical work taken from a $\pm$250 kVAr and a $\pm$75 kVAr static compensator.

II. Average Modeling Principles

State-space averaging (SSA) was established by Middlebrook and Cuk [4], and has been widely used for modeling dc–dc converters. The time-piecewise state equations are averaged over a switching cycle to give a continuous-time description. Essentially SSA assumes that the averaged state equations will give waveforms that are close to the averaged exact waveforms. This is true only at zero perturbation frequency, and when perturbations approach the switching frequency the error is ill defined. In classical SSA, the switching frequency is absent from the average model, while it is clearly an important parameter of a real system. However, in [5] a switching-frequency dependent average model for dc–dc converters was proposed, giving more accurate results than standard SSA.

To put averaging on a firmer basis, a review in [6] surveyed the Bogoliubov theorem for finding a bound for approximation of the time-varying state equation by averaging. It

Manuscript received July 1, 2007; revised September 6, 2007. Recommended for publication by Associate Editor J. Enslin.

M. T. Bina is with the Faculty of Electrical Engineering, K. N. Toosi University of Technology, Tehran 14317, Iran (e-mail: tavakoli@kntu.ac.ir).

A. K. S. Bhat is with the Department of Electrical and Computer Engineering, University of Victoria, Victoria, BC V8W 3P6, Canada (e-mail: bhat@ece.uvic.ca).

Digital Object Identifier 10.1109/TPEL.2007.915174

also described the Krylov–Bogoliubov–Mitropolskii (KBM) method for finding the approximation error. The averaging theory discussed in [6] has been extended to cases in which state discontinuities occur [7]. A general feedback pulsewidth modulation (PWM) was discussed based on an integral form of the state equations rather than the standard differential form. A theorem was proved to this effect: for an arbitrarily large but bounded time interval and a sufficiently small switching period, the exact system and its average model can remain arbitrarily close to each other [7]. Moreover, if the average model tends to an asymptotically stable equilibrium point, the theorem can be extended to an infinite time interval [8]. Furthermore, multi-frequency averaging of dc–dc converters are introduced in [9], and synthesis of averaged circuit models for switched power converters are discussed in [10].

A. Application to AF or STATCOM

Consider an AF or STATCOM connected to a power system. When operated in open loop, the switching transitions occur at predetermined times. However, when the shunt device is embedded in a control loop, the transitions will occur at times determined by the state variables themselves. With this in mind, the open-loop average equations are obtained in a standard form that can later be modified for closed-loop control

$$\dot{\mathbf{X}}(t) = f(\mathbf{X}(t), \mathbf{s}(t), \mathbf{u}(t)) \tag{1}$$

where $\mathbf{X}(t)$ is the state vector, $\mathbf{u}(t)$ is the input vector and $\mathbf{s}(t) = [s_a(t), s_b(t), s_c(t)]^T$ is the vector of switching function. Note that at this stage we do *not* consider the duty ratio to be a continuous function of time, but rather a discrete value associated with an individual switching period. We now apply the averaging operator [11]

$$\xi_a(t) = \text{average}\, \xi(t) \triangleq \frac{1}{T_C} \int_{t-T_C}^{t} \xi(\tau) d\tau \tag{2}$$

to (1) over $[t - T_C, t]$, to get an average model described by

$$\dot{\mathbf{X}}_a(t) = g(\mathbf{X}_a(t), \bar{\mathbf{s}}(t), \mathbf{u}(t)) \tag{3}$$

where $\mathbf{X}_a(t)$ is the average state vector, and $\bar{\mathbf{s}}(t)$ is the approximate continuous averaged switching function in connection with the approximate continuous duty ratio $\mathbf{D}(t)$. This new vector $\bar{\mathbf{s}}(t)$ is a continuous function of time that is controlled by the AF or STATCOM. Additionally, the developed averaged model of (3) can be further identified using a neural network to be simulated very fast with EMTP-like simulators for single-frequency applications in power systems. From (1) and (3) it can easily be shown that [11]

$$\begin{aligned} &\|\mathbf{X}(t) - \mathbf{X}_a(t)\| \\ &\quad \le \|\mathbf{X}(0) - \mathbf{X}_a(0)\| + \left\| \int_0^t [f(\mathbf{X}(\tau), \mathbf{s}(\tau), \mathbf{u}(\tau)) \right. \\ &\qquad \left. - g(\mathbf{X}_a(\tau), \bar{\mathbf{s}}(\tau), \mathbf{u}(\tau))] d\tau \right\|. \end{aligned} \tag{4}$$

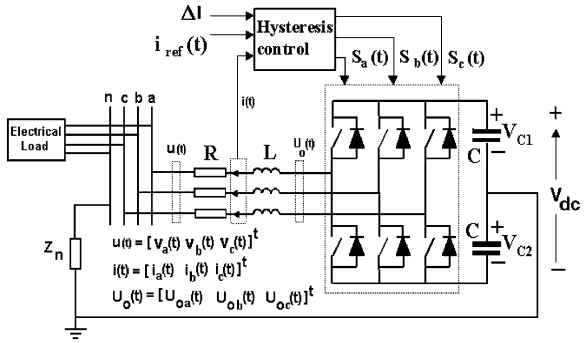

Fig. 1. Three-phase shunted AF or STATCOM.

Starting from (4), a theorem in [4] describes the closeness of $\mathbf{X}(t)$ and $\mathbf{X}_a(t)$. Assume δ, M, T_0 and K are positive real values. For any small δ and large $M > t_0$ (take $t_0 = 0$ here), there exists a T_0 (a function of δ and M) and a positive constant K such that for switching period $T_C \in [0, T_0]$

$$\|\mathbf{X}(t) - \mathbf{X}_a(t)\| \le (\|\mathbf{X}(0) - \mathbf{X}_a(0)\| + \delta) e^{KM}. \tag{5}$$

Now let $\mathbf{X}(0) = \mathbf{X}_a(0)$. Equation (5) says that for any bounded time interval, $\mathbf{X}(t)$ and $\mathbf{X}_a(t)$ can remain close to each other, provided the switching period is small enough. Another theorem in [4] states if $\mathbf{X}_a(t)$ approaches an asymptotically stable equilibrium point, then there exists a sufficiently small T_0 (a function of δ) such that for switching period $T_C \in [0, T_0]$, $\|\mathbf{X}(t) - \mathbf{X}_a(t)\| \le \delta$. Therefore, if the averaged model is asymptotically stable, which is generally true, $\mathbf{X}(t)$ will be very close to $\mathbf{X}_a(t)$. As the low frequency 50/60 Hz sinusoidal utility voltages vary slowly compared to the high averaging frequency, these theorems validate the averaging approach to modeling AF or STATCOM [11].

III. Variable Switching Frequency Model

Fig. 1 shows a three-phase AF or STATCOM, comprising a voltage-sourced inverter connected through an inductance in series with a transformer to a stiff power-system bus [12]–[15]. In principle, the leakage inductance of the coupling transformer might be used in FACTS devices as the commutation inductance. The capacitors carry the dc levels V_{C1} and V_{C2}, where $V_{\rm DC} = V_{C1} + V_{C2}$. The converter current can be controlled to emulate a certain application. Extracting different strategies for reference currents as well as applications of shunt active power filters are examined in [12]–[19]. Here the hysteresis current-controlled strategy is considered for high power shunt AF or STATCOM to keep the instantaneous error between the reference current $\mathbf{i}_{\rm ref}$ and the actual current $\mathbf{i}$ within a band of width $\pm\Delta I/2$. If ΔI is kept constant, a variable modulation frequency is produced that is analyzed in this section.

A. State-Space Model

In this section we apply the foregoing methodology to develop an average model of AF or STATCOM, shown in Fig. 1.

There are two topological modes for every leg. The state equations for the two modes can be obtained separately then, introducing the switching function $s(t) \in [-1, 1]$, combined into a single state equation

$$\dot{\mathbf{X}}(t) = (\mathbf{A}_0 + \mathbf{A}_1 s_a(t) + \mathbf{A}_2 s_b(t) + \mathbf{A}_3 s_c(t))\mathbf{X}(t) + \mathbf{b}\mathbf{u}(t) \quad (6)$$

$$\mathbf{A}_0 = \begin{bmatrix} -\frac{R}{L}[\mathbf{I}]_{3\times 3} & -\frac{1}{2L}[\mathbf{1}]_{3\times 2} \\ \frac{1}{2C}[\mathbf{1}]_{2\times 3} & [\mathbf{0}]_{2\times 2} \end{bmatrix},$$

$$\mathbf{A}_k = \begin{bmatrix} [\mathbf{0}]_{3\times 3} & -\frac{1}{2L}[\mathbf{J}_k]_{3\times 2} \\ \frac{1}{2C}[\mathbf{J}_k]^T_{2\times 3} & [\mathbf{0}]_{2\times 2} \end{bmatrix}$$

$$\mathbf{b} = \begin{bmatrix} \frac{1}{L} & 0 & 0 \\ 0 & \frac{1}{L} & 0 \\ 0 & 0 & \frac{1}{L} \\ 0 & 0 & 0 \\ 0 & 0 & 0 \end{bmatrix}, \quad \mathbf{X}(t) = \begin{bmatrix} i_a(t) \\ i_b(t) \\ i_c(t) \\ V_{C1}(t) \\ V_{C2}(t) \end{bmatrix},$$

$$\mathbf{u}(t) = \begin{bmatrix} v_a(t) \\ v_b(t) \\ v_c(t) \end{bmatrix},$$

$$k = 1, 2, 3 \quad (6a)$$

where $[\mathbf{I}]$ is the unit matrix, $[\mathbf{0}]_{M\times N}$ is an $M \times N$ matrix of zeros, $[\mathbf{1}]_{M\times N}$ is an M—by—N matrix of ones, and the kth row of $[\mathbf{J}_k]_{3\times 2}$ is equal to $[1, -1]$ while its four other entries are zero. Then (6) is averaged over a switching period to develop a continuous-time model, in the form of (3). Applying the averaging operator of (2), let $\mathbf{X}_a(t)$, the averaged state vector, be defined as

$$\mathbf{X}_a(t) = \frac{1}{T_C}\int_{t-T_C}^{t} \mathbf{X}(\tau)d\tau. \quad (7)$$

Now, it can be shown that [11]

$$\dot{\mathbf{X}}_a(t) = \frac{1}{T_C}\int_{t-T_C}^{t} \frac{d\mathbf{X}(\tau)}{d\tau}d\tau. \quad (8)$$

Integrating (6) over $[t - T_C, t]$ and applying (7) and (8), we get

$$\dot{\mathbf{X}}_a(t) = \mathbf{A}_0\mathbf{X}_a(t) + \mathbf{A}_1\frac{1}{T_C}\int_{t-T_C}^{t} s_a(\tau)\mathbf{X}(\tau)d\tau + \mathbf{A}_2\frac{1}{T_C}\int_{t-T_C}^{t} s_b(\tau)\mathbf{X}(\tau)d\tau + \mathbf{A}_3\frac{1}{T_C}\int_{t-T_C}^{t} s_c(\tau)\mathbf{X}(\tau)d\tau + \mathbf{b}\frac{1}{T_C}\int_{t-T_C}^{t} \mathbf{u}(\tau)d\tau. \quad (9)$$

Here, T_C is the averaging period, which should be determined. Note that because the switching frequency is variable, it is essential to decide on the value of T_C. Hence, we approximate a triangular behavior for the ripples of actual current as shown by Fig. 2. Further, the effect of losses (R) is neglected, and the converter output voltages $u_{oj}(j = a, b, c)$ has a rectangular waveform of amplitudes V_{C1} and $-V_{C2}$ with a variable period of $T_{\rm sw}$. The durations of positive and negative pulses are $T_{\rm sw1}$ and $T_{\rm sw2}$, respectively, $(T_{\rm sw} = T_{\rm sw1} + T_{\rm sw2})$. Meanwhile, the converter average voltage u_{oav} is assumed constant during a modulation period. In the case that $V_{C1} = V_{C2} = V_{\rm dc}/2$, using Fig. 2, it can be shown that (see Appendix 1 for details)

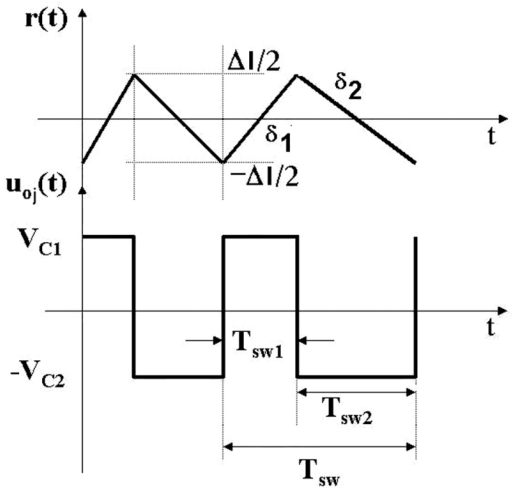

Fig. 2. Approximate linearized ripple along with the converter exact voltage.

$$T_{\rm sw} = \frac{2L\Delta I}{\frac{V_{\rm dc}}{2}\left(1 - \left(\frac{u_{oav}}{\frac{V_{\rm dc}}{2}}\right)^2\right)} = \frac{4L\Delta I}{V_{\rm dc}\left(1 - \left(\frac{2u_{oav}}{V_{\rm dc}}\right)^2\right)} \quad (10)$$

where the switching period $T_{\rm sw}$ is variable, if ΔI is constant. Using the explained theorems on closeness of $\mathbf{X}(t)$ and $\mathbf{X}_a(t)$, the averaging period T_C is assumed less than or equal to the minimum of $T_{\rm sw}$ as follows:

$$T_C \le \min_{u_{oav}=0} T_{\rm sw} = \frac{2L\Delta I}{\frac{V_{\rm dc}}{2}} = \frac{4L\Delta I}{V_{\rm dc}}. \quad (11)$$

The waveform of $s(\tau)$ during $[t - T_C, t]$ has six possible forms, as shown in Fig. 3. Each of these forms can be substituted as the switching functions in the right hand side of (9). A detailed analysis was done by expanding the corresponding Taylor series, and taking the worst case leads us to

$$\frac{1}{T_C}\int_{t-T_C}^{t} s_j(\tau)\mathbf{X}(\tau)d\tau = \bar{s}_j(t)\mathbf{X}_a(t) + \frac{\dot{\mathbf{X}}(t)T_C}{2} \quad j = a, b, c. \quad (12)$$

Here, $\bar{s}_j(t) = (2t_{{\rm on},j}(t) - 1)/T_C$ is the average switching function, where $t_{{\rm on},j}(t)$ is the sub-interval of $[t - T_C, t]$ during which the jth phase $(j = a, b, c)$ upper switch is closed. If the average of $\mathbf{X}(t)$ taken over T_C is close to its average taken over the sub-intervals shown by Fig. 3, the error term in (12), $(\dot{\mathbf{X}}(t)T_C)/(2)$, will be negligible (see Appendix 2 for more details). The slower the variation of $\mathbf{X}(t)$ and lower the averaging period T_C, the smaller the error. This is true for power-systems

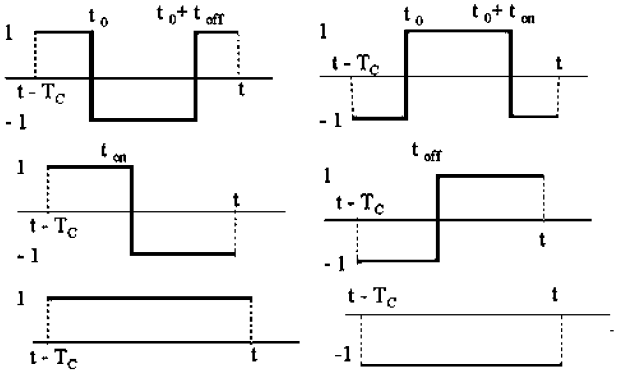

Fig. 3. Six possible forms of $s(\tau)$ over $[t-TC, t]$.

applications in which the averaging frequency is much bigger than the synchronous frequency, resulting in a slow variation of $\mathbf{X}(t)$ during an averaging period. The switching function average in Fig. 3 over $[t-T_C, t]$, for all possible cases, is

$$\frac{1}{T_C}\int_{t-T_C}^{t} s_j(\tau)d\tau = 2D_j(t)-1 \qquad j=a,b,c \quad (13)$$

introducing a continuous duty-ratio function $D_j(t)$. Hence, the resultant averaged state equation is

$$\begin{aligned}\dot{\mathbf{X}}_a(t) &= (\mathbf{A}_0 + \mathbf{A}_1(2D_a(t)-1) \\ &\quad + \mathbf{A}_2(2D_b(t)-1) \\ &\quad + \mathbf{A}_3(2D_c(t)-1))\mathbf{X}_a(t) + \mathbf{b}\bar{\mathbf{u}}(t) \end{aligned} \quad (14)$$

where $\bar{\mathbf{u}}(t)$ is the average of the input vector $\mathbf{u}(t)$. In practice, duty ratio is positive for all t. For the hysteresis current reference vector $\mathbf{i}_{\rm ref}$, the converter reference voltage is

$$u_{oj-\rm ref}(t) = L\frac{di_{j\rm ref}(t)}{dt} + Ri_{j\rm ref}(t) + v_j(t) \qquad j=a,b,c. \quad (15)$$

Dividing $u_{oj-\rm ref}$ by $(V_{\rm dc}/2)$ gives a switching reference, which is substituted in (13) to get three continuous duty ratios $D_a(t), D_b(t)$ and $D_c(t)$. It is noticeable that $(di_{j\rm ref}(t))/(dt)$ can be mathematically subjected to error, and this error can be technically lowered. Nevertheless, in circuit simulators (e.g., PSpice), (15) can be modeled using a current-dependent current-source of $i_{j\rm ref}(t)$ that is connected through an inductance L and a resistance R to an independent voltage source of v_j. Thus, the voltage across the current-dependent current-source presents the desired voltage reference $u_{oj-\rm ref}$. Alternatively, this can be done using the available outcome of the modulator $(s_j(t))$ that is integrated like (13) (see Section V and Fig. 12 for more explanation).

B. Average Circuit Model

Five states of (14) describe the average inductor currents and capacitor voltages. The first three equations can be interpreted as meaning that the average inductor current of each phase depends on the voltage difference between the utility and a voltage-controlled voltage source (VCVS). These three VCVS are named $u_{oav-j}(t)(j=a,b,c)$, and obtained by comparing the first three equations of (14) with (15) as follows:

$$u_{oav-j}(t) = V_{C1}(t)\frac{1+\bar{s}_j(t)}{2} - V_{C2}(t)\frac{1-\bar{s}_j(t)}{2} \qquad j=a,b,c \quad (16)$$

The fourth equation shows that the current of capacitor C_1 (averaged over every T_C) is the sum of three average currents of upper switches, each can be represented by a current-controlled current source (CCCS) $i_{us-j}(t)(j=a,b,c)$. The fifth equation similarly defines the average current of capacitor C_2 as the sum of three average currents of lower switches $(i_{ls-j}(t), j=a,b,c)$, forming six CCCS in total:

$$\begin{cases} i_{us-j}(t) = i_j\frac{1+\bar{s}_j(t)}{2} \\ i_{ls-j}(t) = i_j\frac{1-\bar{s}_j(t)}{2} \end{cases} \qquad j=a,b,c. \quad (17)$$

The resulting equivalent circuit model is shown in Fig. 4, and is suitable for SPICE-like circuit simulators. A small impedance Z_n connecting the neutral point n to the earth is shown in Fig. 4, which is useful for protection design of the STATCOM.

C. Ripple Estimation

The difference between the state vectors of the exact and average models is the switching ripple vector $\mathbf{r}(t)$ (plus any residual error in the average model) expressed by $\mathbf{r}(t) = \mathbf{X}(t) - \mathbf{X}_a(t)$. We can consider $\mathbf{r}(t)$ being the state vector of a ripple model. Taking (6) and (14), the state equation of the ripple model can be obtained and solved to provide a perfect correction to the average model. However, this is computationally equivalent to solving the exact model itself. In practice, some useful economies can be made. Considering Fig. 1, writing two KVLs for the actual current vector $\mathbf{i}$ during $T_{\rm sw1}$ and $T_{\rm sw2}$ [similar to (15)], combining with a KVL for the average current and ignoring R will provide an approximate ripple on top of the average currents. Then, using the resulting ripples for the phase currents, the capacitor voltage ripples are obtained. Thus, by doing a detailed analysis, the ripple vector can be given as (18), shown at the bottom of the next page, where r_a, r_b, and r_c are three switching ripples of the AF or STATCOM currents, r_{C1} and r_{C2} are the ripples of the two capacitor dc voltages. Adding the approximate $\mathbf{r}(t)$ to the average waveform $\mathbf{X}_a(t)$ gives waveforms that are usefully close to the exact ones. We call this the average-plus-ripple model.

D. Simulation and Experimental Results

In this section we compare various simulation results for our models, performed with MATLAB and PSpice. The parameters used here are based on those of a ± 250 kVAr practical STATCOM, providing good agreement with the performed simulations. The three-phase input voltages were $\mathbf{u}(t) = 311[\cos(\omega t+\pi/2), \cos(\omega t+\pi/2-2\pi/3), \cos(\omega t+\pi/2+2\pi/3)]^T$, and $L = 0.6$ mH, $C_1 = C_2 = 1.2$ mF, $R = 0.04\ \Omega$. The reference current vector was $\mathbf{i}_{\rm ref}(t) = I_m[\sin(\omega t+\theta), \cos(\omega t+\theta-2\pi/3), \cos(\omega t+\theta+2\pi/3)]^T$, and

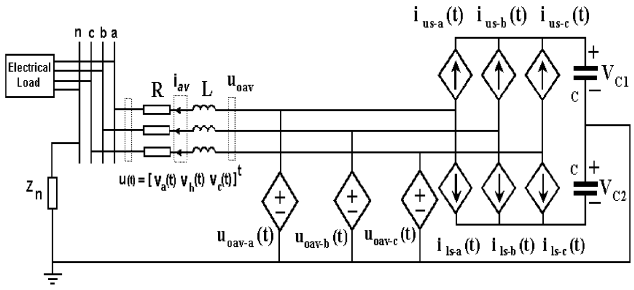

Fig. 4. Equivalent average circuit model for shunt applications, suitable for SPICE-like circuit simulators.

the hysteresis half-band was 8 A. The following simulations have been performed.

1) Steady state: An inductive case with reference parameters $I_m = 50$ A and $\theta = 0$ was simulated with PSpice using the average circuit model (see Fig. 4), comparable with those of experimental three-phase currents absorbed by the compensator. Fig. 5(a)–(b) show the waveforms.
2) Harmonic absorption: A simple filtering example was simulated with PSpice using the average circuit model. The shunt device absorbs reactive current with reference parameters $I_m = 10$ A and $\theta = 0$, being distorted by fifth harmonic current that is about 7.5% of its fundamental reactive current. Fig. 5(c)–(d) present the three-phase currents concerned with both the averaged simulation and the experimental results.
3) Ripple estimation: The average-plus-ripple model was employed to add the ripples on top of the three-phase currents with MATLAB. Fig. 5(e) shows the simulation results, and the shapes can be compared with those of the practical case illustrated by Fig. 5(f). The hysteresis half-band used in the simulation was 8 A since a small band provides the possibility of showing high-frequency ripple simulations. Whereas, the experimental results are obtained with a hysteresis half-band much higher than 8 A with a lower switching frequency in order to reduce the losses. For theoretical modeling and design, experimental results are not necessarily needed.

The equivalent circuit model of Fig. 4, simulated with PSpice [Fig. 5(a), (c)], demonstrates the compatibility of the average model for the involved perturbation frequency. Simulation results given by Fig. 5(a) and (c) introduce waveforms so that their shapes can be compared with those of experimental outcomes of Fig. 5(b) and (d), respectively. Ignoring the high switching frequency ripples the average simulations are in good agreement with those of the exact practical results, validating the average circuit model as well as the mathematical average model. Simulation results obtained by the average-plus-ripple model in Fig. 5(e) are very close to the exact hysteresis waveforms in Fig. 5(f), validating the average-plus-ripple model. But the developed average models ran much faster than the exact model (our PSpice simulations confirm that when the time step for the exact system has to be small, then the average models perform at least 60 times faster than the exact system simulations), offering useful savings in situations where extremely accurate waveforms are not important (e.g., for investigating the effects of three-phase unbalance on the operation of STATCOM or AF).

IV. Fixed Switching Frequency Model

Fig. 6(a) shows an isolated three-phase STATCOM, controlled by a PWM scheme [20]. The capacitor carries the dc voltage $V_{\rm dc}$, $\mathbf{v}$ is the power system voltage and converter composed voltage is $\mathbf{u}_o$. By varying $\mathbf{u}_o$, reactive power can be controlled to emulate a certain application such as voltage regulation. In a STATCOM, there is a small phase difference (α) between the converter voltage and the ac system voltage. In other words, current that flows through STATCOM contain both reactive and active components. In fact, changing α will vary the dc voltage $V_{\rm dc}$, and consequently the converter output $\mathbf{u}_o$. In [21], [22], the explained mode of operation is modeled by transforming the STATCOM state equations to a synchronous frame, showing a stable system with oscillatory dynamic response for the STATCOM.

A typical steady state operation of STATCOM as a function of α is depicted in Fig. 6(b). Three state variables i_d, i_q and $V_{\rm dc}$ give the equivalent active current, reactive current, and dc voltage, respectively. This figure shows almost a linear relationship for the reactive current i_q as a function of α over $[-1.5^o, 1.5^o]$, although the state equations represent a nonlinear system. When α is negative, STATCOM works in capacitive mode, while positive α corresponds to inductive mode. This suggests a way of controlling STATCOM, mainly by α.

Note that the control loop focuses on α to get the required operational setting points [see Fig. 6(b)], while the PWM modulation index is fixed close to one. In other words, the converter voltage is varied by control parameter α over the linear region. Thus, there are two main periods involved in STATCOM: the reference period T_R (obtained from the mains supply frequency) and the switching period T_C (depending on T_R), the period of the PWM carrier, typically a few kilohertz. As is usual in PWM,

$$\mathbf{r}(t) = \begin{cases} r_j(t)(j=a,b,c) = \begin{cases} \frac{V_{C1}}{L}\left(T_{\mathrm{sw1}-j} - \int_{t}^{t+T_{\mathrm{sw1}-j}} \frac{u_{oav-j(\tau)}}{V_{C1}} d\tau\right): & t \le \tau \le t + T_{\mathrm{sw1}-j} \\ \frac{-V_{C2}}{L}\left(T_{\mathrm{sw2}-j} + \int_{t+T_{\mathrm{sw1}-j}}^{t+T_{\mathrm{sw}-j}} \frac{u_{oav-j(\tau)}}{V_{C2}} d\tau\right): & t + T_{\mathrm{sw1}-j} \le \tau \le t + T_{\mathrm{sw}-j} \end{cases} \\ \begin{cases} r_{C1} = \sum_{j=a,b,c} r_j(t) \frac{1+\bar{s}_j(t)}{2} \\ r_{C2} = \sum_{j=a,b,c} r_j(t) \frac{1-\bar{s}_j(t)}{2} \end{cases} \end{cases} \tag{18}$$

$T_R \gg T_C$. Further, it is assumed that T_R is an integer multiple of T_C : $T_R = MT_C$. We define

$$s(t) = \sum_{n=1}^{m} S_n(t) \tag{19}$$

$$S_n(t) = \begin{cases} 1 & (n-1)T_C < t \le [n-1+D(nT_C)]T_C \\ -1 & [n-1+D(nT_C)]T_C < t \le nT_C \\ 0 & \text{otherwise} \end{cases} \tag{20}$$

where $S_n(t)$ is the switching function within the nth switching period and $D(nT_C)$ is the duty ratio for the nth switching period. Note again that, at this stage, the duty ratio is considered as a discrete value associated with an individual switching period.

A. State-Space Model

Consider the STATCOM of Fig. 6(a). Applying the method of Section III-A, and introducing the switching function $s(t) \in [-1, 1]$, the state equations can be obtained

$$\dot{\mathbf{X}}(t) = (\mathbf{A}_r + \mathbf{A}_a s_a(t) + \mathbf{A}_b s_b(t) + \mathbf{A}_c s_c(t))\mathbf{X}(t) + \mathbf{b}\mathbf{v}(t) \tag{21}$$

$$\mathbf{A}_r = \begin{bmatrix} \frac{-R}{L} & 0 & 0 \\ 0 & \frac{-R}{L} & 0 \\ 0 & 0 & 0 \end{bmatrix}, \quad \mathbf{A}_a = \begin{bmatrix} 0 & 0 & \frac{1}{3L} \\ 0 & 0 & \frac{-1}{6L} \\ \frac{-1}{2C} & 0 & 0 \end{bmatrix},$$

$$\mathbf{A}_b = \begin{bmatrix} 0 & 0 & \frac{-1}{6L} \\ 0 & 0 & \frac{1}{3L} \\ 0 & \frac{-1}{2C} & 0 \end{bmatrix},$$

$$\mathbf{A}_c = \begin{bmatrix} 0 & 0 & \frac{-1}{6L} \\ 0 & 0 & \frac{-1}{6L} \\ \frac{1}{2C} & \frac{1}{2C} & 0 \end{bmatrix}, \quad \mathbf{b} = \begin{bmatrix} \frac{-2}{3L} & \frac{1}{3L} & \frac{1}{3L} \\ \frac{1}{3L} & \frac{-2}{3L} & \frac{1}{3L} \\ 0 & 0 & 0 \end{bmatrix},$$

$$\mathbf{X}(t) = \begin{bmatrix} i_a(t) \\ i_b(t) \\ V_{\rm dc}(t) \end{bmatrix}, \mathbf{v}(t) = \begin{bmatrix} v_a(t) \\ v_b(t) \\ v_c(t) \end{bmatrix}. \tag{21a}$$

Then (21) is averaged over a switching period to develop a continuous-time model, in the form of (3). Let $\mathbf{X}_a(t)$ and $\dot{\mathbf{X}}_a(t)$, the averaged state vector and its derivative, be considered as in (7) and (9), respectively. Note that here the switching period T_C is fixed. Integrating (21) over $[t - T_C, t]$ and applying (7) and (9), we get

$$\begin{aligned} \dot{\mathbf{X}}_a(t) = \mathbf{A}_r\mathbf{X}_a(t) &+ \mathbf{A}_a\frac{1}{T_C}\int_{t-T_C}^{t} s_a(\tau)\mathbf{X}(\tau)d\tau \\ &+ \mathbf{A}_b\frac{1}{T_C}\int_{t-T_C}^{t} s_b(\tau)\mathbf{X}(\tau)d\tau \\ &+ \mathbf{A}_c\frac{1}{T_C}\int_{t-T_C}^{t} s_c(\tau)\mathbf{X}(\tau)d\tau \\ &+ \mathbf{b}\frac{1}{T_C}\int_{t-T_C}^{t} \mathbf{v}(\tau)d\tau. \end{aligned} \tag{22}$$

The waveform of $s(\tau)$ during $[t-T_C, t]$ has four possible forms, as shown in Fig. 7. Each of these forms can be substituted in the right hand side of (22) as the switching waveform. Taking the worst case leads us to

$$\begin{aligned} \frac{1}{T_C}\int_{t-T_C}^{t} s_j(\tau)\mathbf{X}(\tau)d\tau &= (2D_j(t)-1)\mathbf{X}_a(t) + \frac{\dot{\mathbf{X}}(t)T_C}{2} \\ & j = a, b, c. \end{aligned} \tag{23}$$

Here, $D_j(t) = t_{{\rm on},j}(t)/T_C$, where $t_{{\rm on},j}(t)$ is the sub-interval of $[t - T_C, t]$ during which the upper switch is closed. Again, the slower is the variation of $\mathbf{X}(t)$ and higher is the PWM frequency, the smaller is the error (see Appendix 2 for more details). Since the power-system frequency is much smaller than the PWM frequency, the error term is expected to be small. Integrating the PWM switching functions in Fig. 7 over $[t - T_C, t]$, the switching function average is

$$\frac{1}{T_C}\int_{t-T_C}^{t} s_j(\tau)d\tau = 2D_j(t) - 1 \quad j = a, b, c \tag{24}$$

giving the continuous duty-ratio function $D_j(t)$. The resultant average state equation is

$$\begin{aligned} \dot{\mathbf{X}}_a(t) = (\mathbf{A}_r &+ \mathbf{A}_a(2D_a(t)-1) \\ &+ \mathbf{A}_b(2D_b(t)-1) \\ &+ \mathbf{A}_c(2D_c(t)-1))\mathbf{X}_a(t) + \mathbf{b}\bar{\mathbf{v}}(t) \end{aligned} \tag{25}$$

where $\bar{\mathbf{v}}(t)$ is the average of the input vector $\mathbf{v}(t)$. In practice, $D_j(t)$ has a sinusoidal waveform. Here, the special case is considered where the PWM has a carrier waveform that ramps between -1 and 1, and a sinusoidal reference of $m\sin(\omega t - \pi/2)$ for phase a, m being the modulation index. Considering a Fourier series for $s_a(t)$, its fundamental phasor $S_1 = me^{-j\pi/2}$ is substituted in (23) and (24) (the dc term and higher harmonics being neglected), to find the continuous $D_a(t)$ as

$$D_a(t) \approx \frac{1}{2}\left[1 + m\frac{\sin(\pi/M)}{\pi/M}\sin\left(\omega t - \frac{\pi}{M} + \alpha\right)\right] \tag{26}$$

where M is the ratio of the carrier frequency over the mains frequency. Similar approximations could be given for $D_b(t)$ and $D_c(t)$. Note that the phase angle π/M will not be different for three phases when M is chosen as an odd multiple of three. Here $M = 45$ is considered for the installed device. A MATLAB program was written to calculate the error between the exact duty ratio (at $t = nT_C, n = 1, 2, \ldots, M$) and the continuous approximation in (26). For $M = 45$ (e.g., 2.25 kHz carrier, 50 Hz reference), the worst-case error is less than 1.5%.

B. Average Circuit Model

To get the average circuit model, based on available terms within (21) and (25), first two independent voltage sources along with two voltage-controlled voltage sources (VCVS) are defined as follows in (27) and (28), respectively

$$\begin{aligned} &[f_1(\mathbf{v}(t))\ \ f_2(\mathbf{v}(t))]^T \\ &\quad = [2v_a(t) - v_b(t) \\ &\qquad - v_c(t)\ \ 2v_b(t) - v_a(t) - v_c(t)]^T \end{aligned} \tag{27}$$

$$\begin{aligned} &[g_1(\mathbf{D}(t))\ \ g_2(\mathbf{D}(t))]^T \\ &\quad = [V_{\rm dc}(2D_a(t) - D_b(t) \\ &\qquad - D_c(t))\ \ V_{\rm dc}(2D_b(t) - D_a(t) - D_c(t))]^T. \end{aligned} \tag{28}$$

Three state (25) describe the average inductor currents and capacitor voltage. The first two equations can be interpreted

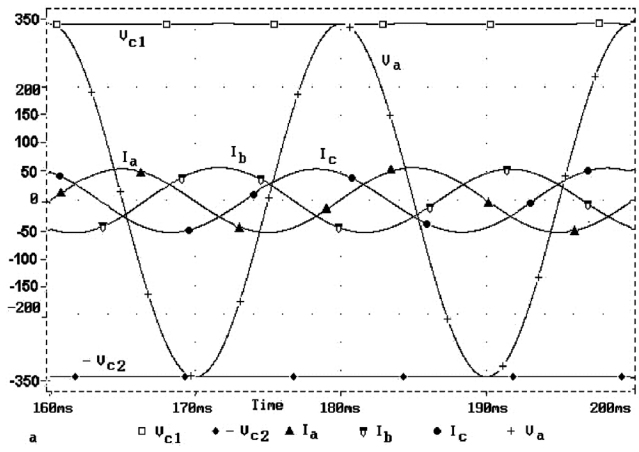

(a)

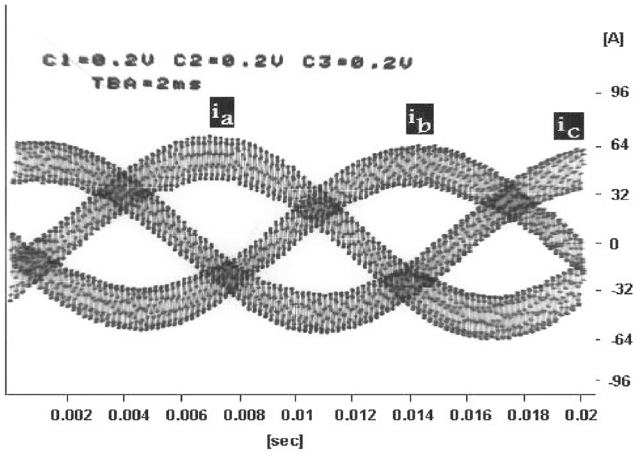

(b)

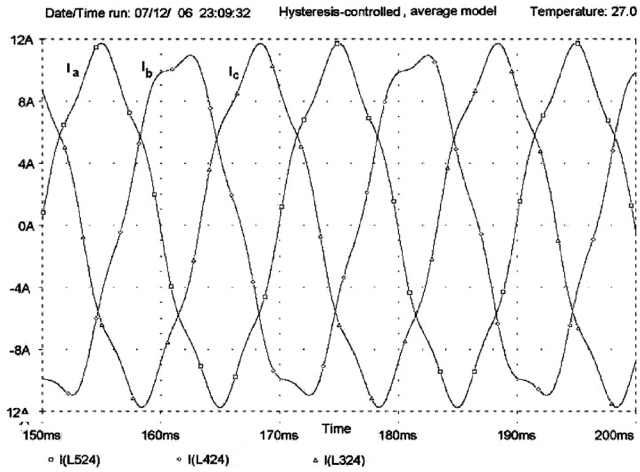

(c)

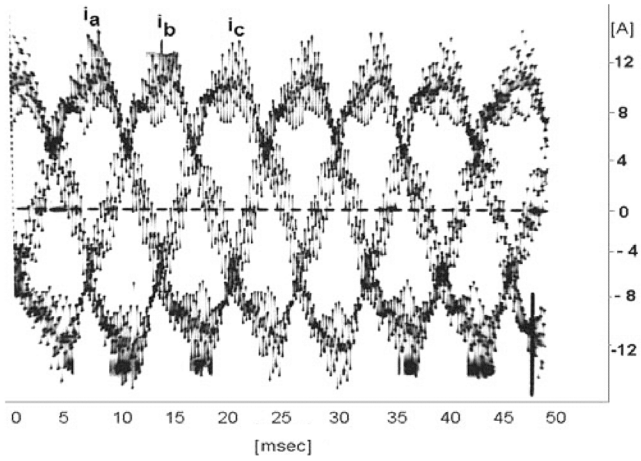

(d)

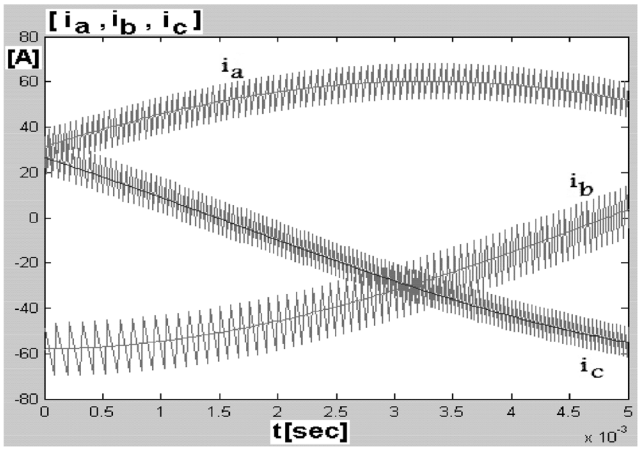

(e)

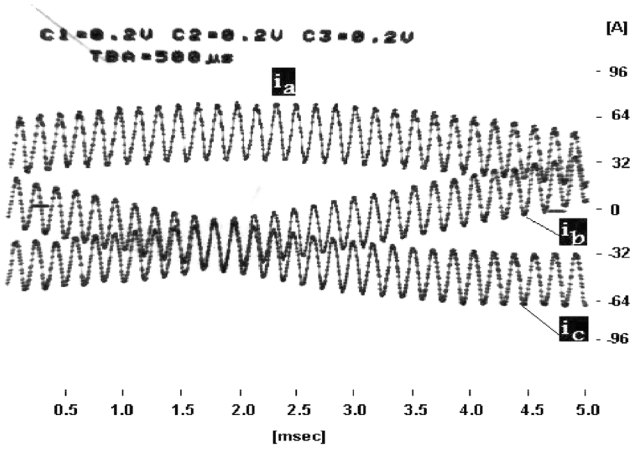

(f)

Fig. 5. Simulation and practical results for the developed average models: (a)–(b) PSpice simulation of an inductive case using the average circuit model compared to the experimental three-phase currents; (c)–(d) PSpice simulation of an active-filter example using the average circuit model, absorbing about 7.5% fifth harmonic on top of the fundamental component, compared to experimental three-phase currents; and (e)–(f) MATLAB adds the ripples on top of the average currents using the average-plus-ripple model compared to the actual currents.

as meaning that the average inductor currents depend on the voltage difference between the independent sources (27) and dependent sources (28).

The third equation shows that the current of capacitor C (averaged over every T_C) is composed of two current-controlled current sources (CCCS) h_1 and h_2, each as a function of duty ratios and line currents, namely

$$[h_1(\mathbf{D}(t), i_a(t))\ \ h_2(\mathbf{D}(t), i_b(t))]^T = [i_a(t)(D_c(t) - D_a(t))\ \ i_b(t)(D_c(t) - D_b(t))]^T. \quad (29)$$

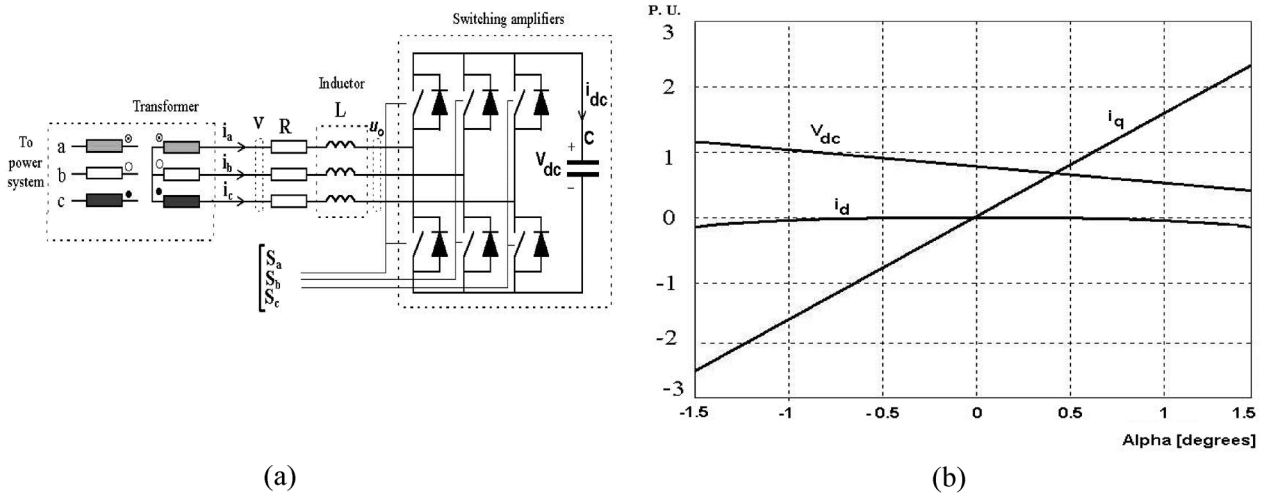

Fig. 6. (a) Equivalent three-phase circuit of STATCOM and (b) equivalent reactive current, active current, and capacitor voltage as a function of α.

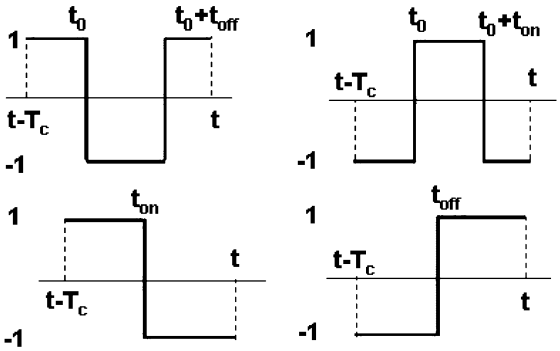

Fig. 7. Four possible forms of $s(\tau)$ over $[t - T_C, t]$.

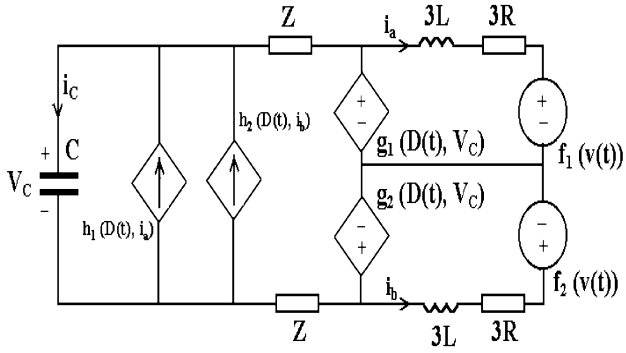

Fig. 8. Equivalent circuit average model of STATCOM, suitable for SPICE-like circuit simulators.

The resulting equivalent circuit model is shown in Fig. 8, and is suitable for circuit simulators such as SPICE. Two big impedances Z connect the capacitor circuit to inductor circuits for PSpice simulation purposes, leaving negligible effect on the circuit behavior.

C. Simulation Results

In this section we compare various simulation results for STATCOM and our models, performed with PSpice (as a circuit simulator) and MATLAB (as a mathematical time domain differential equation simulator). The parameters used here are based on those of an experimental $\pm$75 kVAr STATCOM to validate the proposed models.

1) MATLAB Simulations: First, the average model of STATCOM was simulated. The input voltage was $\mathbf{u}(t) = 155.6[\sin(\omega t + \pi/2), \sin(\omega t + \pi/2 - 2\pi/3), \sin(\omega t + \pi/2 + 2\pi/3)]^T$, and STATCOM parameters are $L = 1.0$ mH, $C_1 = C_2 = 1.2$ mF, $R = 0.06\ \Omega$, and the modulation index was fixed at 0.9. Figs. 9(a) and 10(a) show the state variables of STATCOM for two cases: $\alpha = 1^\circ$ (inductive mode) and $\alpha = -1^\circ$ (capacitive mode). These results show that the capacitor voltage tends to increase for $\alpha = -1^\circ$, while it decreases for $\alpha = 1^\circ$, both converge to certain steady state conditions. The line currents i_a and i_b can be added together to get the other line current i_c.

2) PSpice Simulation Results: The equivalent circuit model of Fig. 8 together with the exact switched-system model of Fig. 6(a) were simulated with PSpice. The parameters are the same as those of MATLAB simulations of Figs. 9 and 10. Figs. 9(b) and 10(b) depict the state variables for both the exact and the average models starting at $t = 120$ ms. Apart from the ripples, the agreement is good, demonstrating the compatibility of the average model for the involved perturbation frequency. The PSpice simulation results can also be compared with those of MATLAB, presented by Figs. 9 and 10. Again the agreement is good, validating the equivalent circuit as well as the mathematical average model.

3) Experimental Result: A $\pm$75 kVAr IGBT-based (SKM200GB124D: 1700 V, 200 A devices) STATCOM was used for experimental tests, with the parameters already given in Section IV-C1. Figs. 9(c) and 10(c) provide a typical STATCOM current along with the capacitor voltage for both inductive and capacitive modes. Comparing PSpice and MATLAB simulations with practical outcomes, the agreement is good, validating the introduced models.

4) An Application Example: As an application of the developed circuit model, here a transient of STATCOM is simulated with PSpice. Initially, the STATCOM is injecting reactive power ($\alpha = -1^\circ$). At t =130 ms, the control angle is changed to

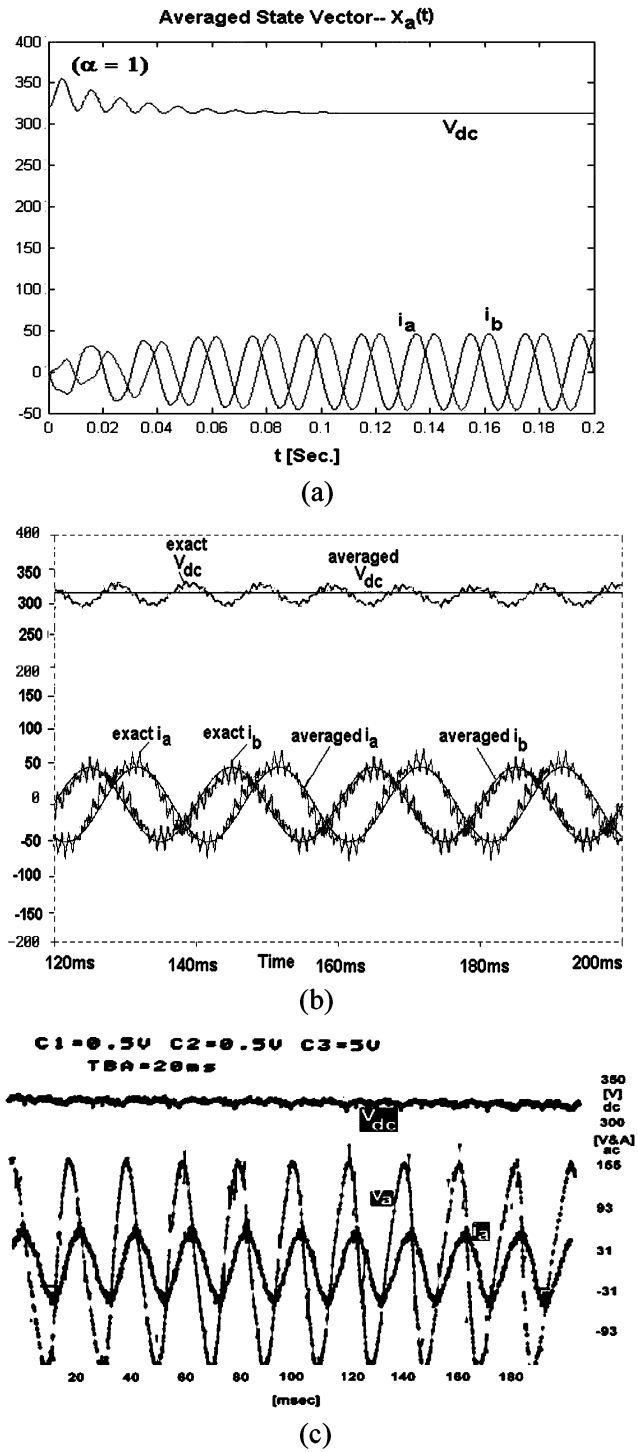

Fig. 9. Simulation results for the average model of STATCOM, operating in an inductive mode ($\alpha = 1^\circ$): (a) MATLAB simulation of the average mathematical model; (b) PSpice simulation of the average and the exact circuit models; and (c) experimental results validating both the simulations and models.

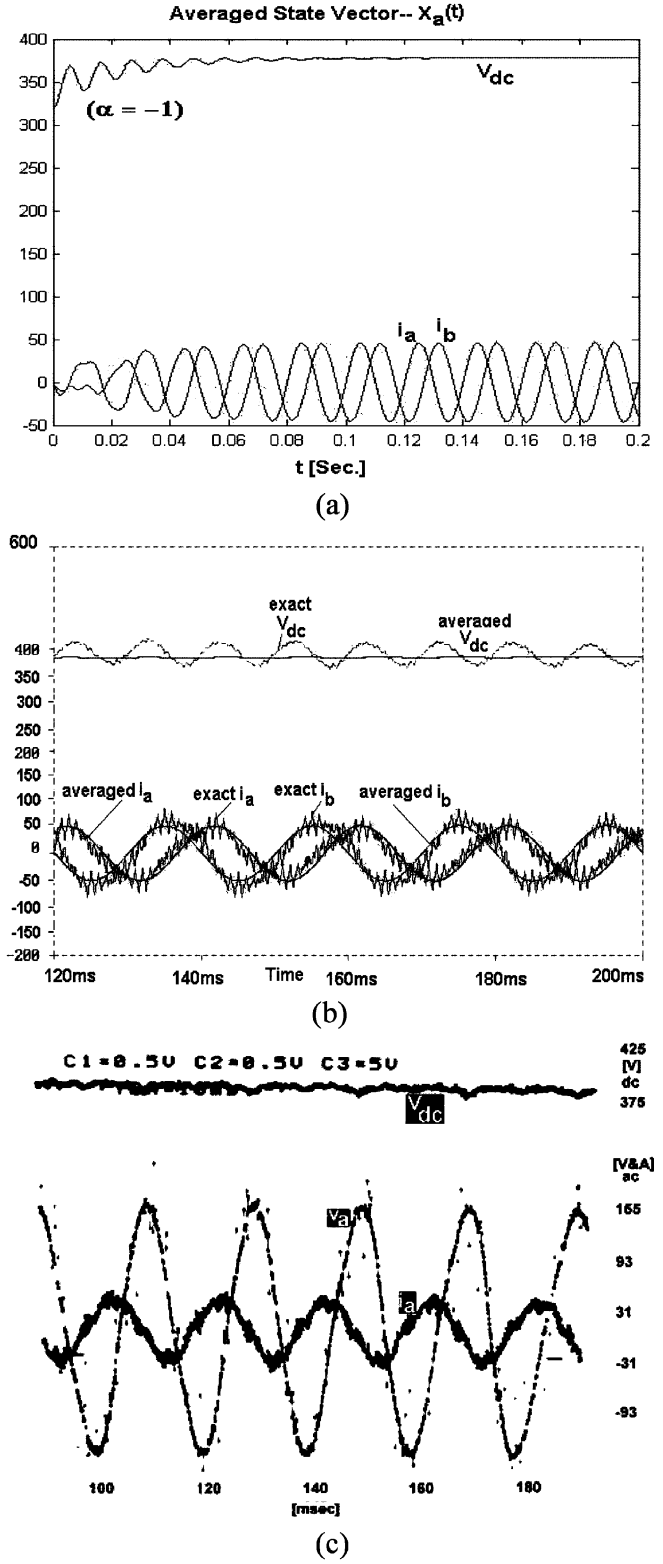

Fig. 10. Simulation results for the average model of STATCOM, operating in a capacitive mode ($\alpha = -1^\circ$): (a) MATLAB simulation of the average mathematical model; (b) PSpice simulation of the average and the exact circuit models; and (c) experimental results validating both the simulations and the models.

$\alpha = 1^\circ$ using a step function, which forces the STATCOM to absorb the same reactive power. Fig. 11(a) shows this simulation, containing both the exact and average waveforms of the capacitor voltage $V_{\rm dc}$ and the inductor current i_a. Also, the applied voltage v_a is included. Similarly, Fig. 11(b) shows experimental results for the transient case, where at about labeled $t =$ 120 ms the same change as that of the simulation case was applied. Comparison of Fig. 11(a)–(b) indicate that both simulation and practical work take about one cycle to approach their new operating points, again validating the average models.

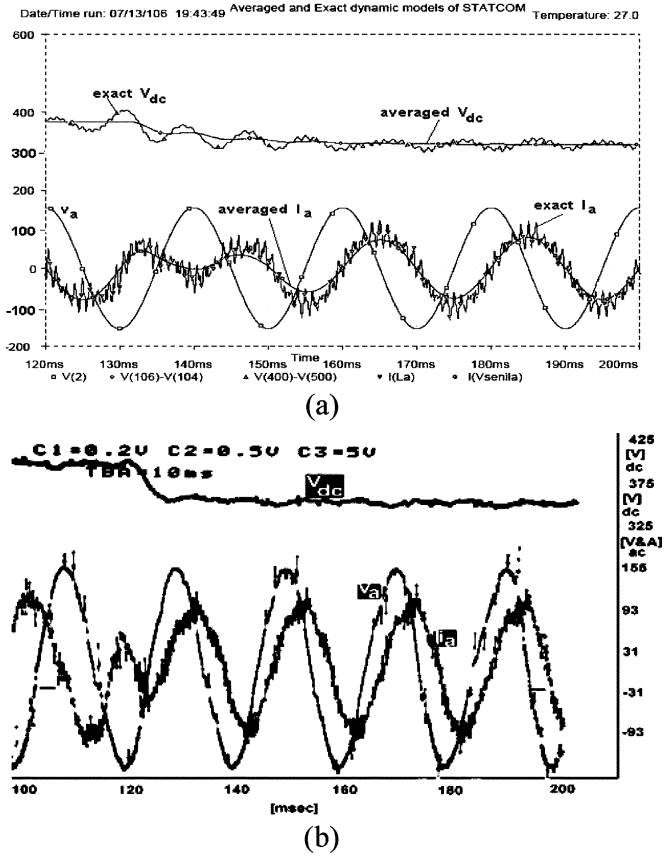

Fig. 11. Transient of STATCOM, changing from a capacitive mode ($\alpha = -1^\circ$) to an inductive mode ($\alpha = 1^\circ$) using a step function: (a) PSpice simulation of both the exact and the average circuit models; and (b) experimental results validating the general shape of the simulations.

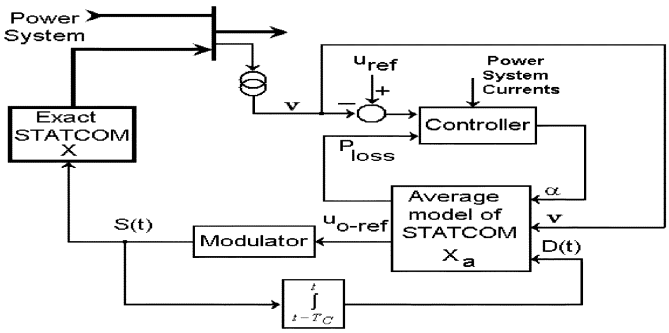

Fig. 12. Typical application of the aveage model in designing the power system voltage controller; where $S(t)$ and $D(t)$ are the vectors of the switching states and the duty ratios, respectively.

V. Control Design Applications

The developed models of (14) and (25) can be used for control design purposes. Duty ratio in (14) is supplied to the model as the switching pulses are modulated by the reference signal. Further, this was embedded in (25) using the sinusoidal modulation of (26) for reactive power control of STATCOM. In practice, embedding the duty ratio is not necessary, and can be managed by the control design and modulating process.

Fig. 12 shows the use of the average model in designing the voltage regulator of a power system bus. Inputs of the average model of (25) are the phase difference α, input vector $\mathbf{v}$ and the vector of duty ratios $D(t)$. The phase angle α is provided by the controller, $\mathbf{v}$ by the power system bus and $D(t)$ is supplied by integrating the outcome of the modulator. Note that bold lines are used to show the power circuit parts while the normal lines present the control diagram.

VI. Conclusion

An average technique has been used to approximate the behavior of power electronic shunt devices connected to a power system, both for variable and fixed switching frequency. Starting with the exact state equations, average mathematical models were developed. Then, equivalent circuit models were derived from the resulting equations. The exact systems (simulated with PSpice and obtained by practical tests) and their approximate models (simulated with MATLAB and PSpice) are all in good agreement. The provided analytical discussions verify that the necessary and sufficient conditions of the averaging theorems in [7] are satisfied by the proposed models. This is further verified by simulation and experimental results.

Appendix I
Variable Switching Period

Consider Fig. 2 to derive the variable expression given by (10). Assume the converter output voltage $(\mathbf{u}_o(t))$ averaged over $[t-T_{\rm sw}, t]$ is $\mathbf{u}_{oav}(t)$. Two slopes δ_1 and δ_2 in Fig. 2 can be worked out as $(\Delta I)/(T_{\rm sw1})$ and $(-\Delta I)/(T_{\rm sw2})$ respectively. In the mean time, by neglecting R, a KVL in Fig. 1 relates $\mathbf{u}_o(t), L$ and $\mathbf{v}(t)$, and another KVL in Fig. 4 relates $\mathbf{u}_{oav}(t), L$ and $\mathbf{v}(t)$ as follows:

$$\begin{cases} \frac{d\mathbf{i}}{dt} = \frac{\mathbf{u}_o(t)-\mathbf{v}(t)}{L} \\ \frac{d\mathbf{i}_{\rm av}}{dt} = \frac{\mathbf{u}_{oav}(t)-\mathbf{v}(t)}{L} \end{cases}. \tag{30}$$

These two equations are then combined together by eliminating $\mathbf{v}(t)$ from (30) to get (using $\mathbf{u}_o(t) = V_{C1} = (V_{\rm dc})/(2)$ or $\mathbf{u}_o(t) = V_{C2} = -(V_{\rm dc})/(2)$ in Fig. 2, i.e., assuming that the capacitor voltages are equal)

$$\begin{cases} \delta_1 = \frac{\frac{V_{\rm dc}}{2}-\mathbf{v}(t)}{L} & \text{during} T_{\rm sw1} \\ \delta_2 = \frac{\frac{V_{\rm dc}}{2}+\mathbf{v}(t)}{-L} & \text{during} T_{\rm sw2} \end{cases} \tag{31}$$

where there exist two approximate expressions for δ_1 that have to be identical. Similarly, this is true for δ_2, leading to

$$\begin{cases} T_{\rm sw1} = \frac{L\Delta I}{\frac{V_{\rm dc}}{2}-\mathbf{u}_{oav}(t)} \\ T_{\rm sw2} = \frac{L\Delta I}{\frac{V_{\rm dc}}{2}+\mathbf{u}_{oav}(t)} \end{cases}. \tag{32}$$

By adding $T_{\rm sw1}$ to $T_{\rm sw2}$, we get an expression for the variable switching period $T_{\rm sw}$ given by (10).

Appendix II
Detailed Average and Error Analysis

Here the details of the error analysis are presented. First, the error term in (12) and (23) is introduced for the possible cases illustrated in Figs. 3 and 7. Second, an upper bound is assigned to the error term. Let $\mathbf{e}(t)$ be the error term. Consider the top left graph in Fig. 3. By substituting its parameters in the second term of (12), we have

$$\frac{1}{T_C}\int_{t-T_C}^{t} s(\tau)\mathbf{X}(\tau)d\tau = \frac{1}{T_C}\left[\int_{t-T_C}^{t_0}\mathbf{X}(\tau)d\tau - \int_{t_0}^{t_0+t_{\text{off}}}\mathbf{X}(\tau)d\tau + \int_{t_0+t_{\text{off}}}^{t}\mathbf{X}(\tau)d\tau\right]. \quad (33)$$

Assuming $t_0 = t - T_C + \gamma$, and $\beta = t - t_0 - t_{\text{off}}$ in this graph, we have $\gamma + \beta = t_{\text{on}} = D(t)T_C$. Also, considering that the integral of $X(t)$ is equal to $Y(t)$, $\int_a^b \mathbf{X}(t)dt = \mathbf{Y}(b) - \mathbf{Y}(a)$, then (33) could be rewritten as

$$\frac{1}{T_C}\int_{t-T_C}^{t} s(\tau)\mathbf{X}(\tau)d\tau = \frac{1}{T_C}[\mathbf{Y}(t) - \mathbf{Y}(t-T_C) - 2\mathbf{Y}(t-\beta) + 2\mathbf{Y}(t-T_C+\gamma]. \quad (34)$$

Now, $\mathbf{Y}(t-T_C), \mathbf{Y}(t-\beta)$, and $\mathbf{Y}(t-T_C+\gamma)$ are expanded by their Taylor series (γ, β, and T_C being very small). For example, $\mathbf{Y}(t-T_C) = \mathbf{Y}(t) - T_C\dot{\mathbf{Y}}(t) + (T_C^2)/(2)\ddot{\mathbf{Y}}(t)$ where the higher terms are ignored as T_C is very small, and $\mathbf{Y}(t)$ is smooth. Substituting these relationships in (34), leads us to the following equation:

$$\frac{1}{T_C}\int_{t-T_C}^{t} s(\tau)\mathbf{X}(\tau)d\tau = \frac{1}{T_C}\left\{\dot{\mathbf{Y}}(t)(2D(t)-1) + \ddot{\mathbf{Y}}(t) \times \left(\frac{-T_C}{2} - (1-D(t))\right)(\gamma - \beta - T_C))\right\}. \quad (35)$$

The first term on the RHS is the average $(\dot{\mathbf{Y}}(t)(2D(t)-1) = \mathbf{X}_a(t)(2D(t)-1)$, and the second term is the error $\mathbf{e}(t)$. A similar procedure was carried out for the other three graphs in Fig. 3. The resulting error functions are

$$\mathbf{e}(t) = \begin{cases} \dot{\mathbf{X}}_a(t)\left(\frac{-T_C}{2} - (1-D(t))\right)(\gamma - \beta - T_C)) \\ \dot{\mathbf{X}}_a(t)\left(\frac{T_C}{2} - D(t)(-\gamma + \beta + T_C)\right) \\ \dot{\mathbf{X}}_a(t)T_C(D(t)^2 - 2D(t) + 1/2) \\ \dot{\mathbf{X}}_a(t)T_C(D(t)^2 - 1/2) \end{cases}. \quad (36)$$

Now an upper bound is assigned to the error function. The error function has different forms as stated in (36). Here it is shown that the error function always obeys $\mathbf{e}(t) \le \dot{\mathbf{X}}(t)(T_C/2)$. Considering the top left graph in Fig. 3, it is clear that $(|\beta-\gamma|)/(T_C) < (t_{\text{on}})/(T_C) = D(t)$. As $1+(\beta-\gamma)/(T_C) \le 1+|(\beta-\gamma)/(T_C)| \le 1+D(t)$, it can easily be found that $\mathbf{e}(t) \le \dot{\mathbf{X}}_a(t)T_C(-D(t)^2+1/2)$. Duty ratio $D(t)$ varies over $[0,1]$, resulting in $-1/2 \le -D(t)^2 + 1/2 \le 1/2$. This implies $\mathbf{e}(t) \le \dot{\mathbf{X}}_a(t)(T_C/2)$. This was also carried out for other graphs, resulting in the same upper bound for all possible cases in the worst case. As a result of this analysis, $\mathbf{e}(t)$ in (12) and (23) is substituted by $\dot{\mathbf{X}}(t)(T_C/2)$.

REFERENCES

[1] C. A. Quinn, N. Mohan, and H. Mehta, "A four-wire current-controlled converter provides harmonic neutralization in three-phase, four wire systems'," in *Proc. IEEE Appl. Power Electron. Conf. (APEC'93)*, 1993, pp. 841–846.

[2] A.-A. Edris *et al.*, "Proposed terms and definitions for flexible ac transmission systems (FACTS)," *IEEE Trans. Power Delivery*, vol. 12, no. 4, pp. 1311–1317, Oct. 1997.

[3] M. T. Bina, M. D. Eskandari, and M. Panahlou, *Design and Installation of a ±25 kVAr D-STATCOM for a Distribution Substation*. Amsterdam, The Netherlands: Elsevier, Mar. 2005, pp. 383–391.

[4] R. D. Middlebrook and S. Ćuk, "A general unified approach to modeling switching-converter power stages," in *Proc. IEEE Power Electron. Spec. Conf.*, 1976, pp. 18–34.

[5] B. Lehman and R. M. Bass, "Switching frequency dependent averaged models for PWM dc–dc converters," *IEEE Trans. Power Electron.*, vol. 11, no. 1, pp. 89–98, Jan. 1996.

[6] P. T. Krein, J. Bentsman, R. M. Bass, and B. C. Lesieutre, "On the use of averaging for the analysis of power electronic systems," *IEEE Trans. Ind. Electron.*, vol. 5, no. 2, pp. 182–190, Apr. 1990.

[7] B. Lehman and R. M. Bass, "Extension of averaging theory for power electronic systems," *IEEE Trans. Power Electron.*, vol. 11, no. 4, pp. 542–553, Jul. 1996.

[8] B. Lehman, J. Bentsman, S. V. Lunel, and E. Verriest, "Vibrational control of nonlinear time lag systems: Averaging theory, stabilizability, and transient behavior," *IEEE Trans. Automat. Control*, vol. 32, no. 3, pp. 509–517, May/Jun. 1996.

[9] V. A. Caliskan, G. C. Verghese, and A. M. Stankovic, "Multifrequency averaging of DC/DC converters," *IEEE Trans. Power Electron.*, vol. 14, no. 1, pp. 124–133, Jan. 1999.

[10] S. R. Sanders and G. C. Verghese, "Synthesis of averaged circuit models for switched power converters," *IEEE Trans. Circuits Syst.*, vol. 38, no. 8, pp. 905–915, Aug. 1991.

[11] M. T. Bina and D. C. Hamill, "Average model of the bootstrap variable inductance," in *Proc. IEEE Power Electron. Spec. Conf. (PESC'00)*, Jun. 2000, [CD ROM].

[12] M. I. M. Montero, E. R. Cadaval, and F. B. Gonzalez, "Comparison of control strategies for shunt active power filters in three-phase four-wire systems," *IEEE Trans. Power Electron.*, vol. 22, no. 1, pp. 229–236, Jan. 2007.

[13] A.-A. Edris, S. Zelingher, L. Gyugyi, and L. J. Kovalsky, "FACTS system studies," *IEEE Power Eng. Rev.*, pp. 4–6, Jun. 2002.

[14] R. Adapa, "FACTS system studies," *IEEE Power Eng. Rev.*, pp. 17–22, Dec. 2002.

[15] H. Fujita and H. Akagi, "Voltage-regulation performance of a shunt active filter intended for installation on a power distribution system," *IEEE Trans. Power Electron.*, vol. 22, no. 3, pp. 1046–1053, May 2007.

[16] A. García-Cerrado, O. Pinzón-Ardila, V. Feliu-Batle, P. Roncero-Sánchez, and P. García-González, "Application of a repetitive controller for a three-phase active power filter," *IEEE Trans. Power Electron.*, vol. 22, no. 1, pp. 237–246, Jan. 2007.

[17] L. Asiminoaei, C. Lascu, F. Blaabjerg, and I. Boldea, "Performance improvement of shunt active power filter with dual parallel topology," *IEEE Trans. Power Electron.*, vol. 22, no. 1, pp. 247–259, Jan. 2007.

[18] N. G. Hingorani and L. Gyugyi, *Understanding FACTS: Concepts and Technology of Flexible ac Transmission Systems*. New York: IEEE Press, 2000, Book.

[19] K. R. Padiyar, *FACTS Controllers in Power Transmission and Distribution*. New Delhi, India: New Age International Publishers (Formerly Wiley Eastern Limited), 2007.

[20] C. D. Schauder, M. Gernhardt, E. Stacey, T. Lemak, L. Gyugyi, T. W. Cease, and A. Edris, "Development of a ±100 MVAR static condenser for voltage control of transmission systems," *IEEE Trans. Power Delivery*, vol. 10, no. 3, pp. 1486–1496, Jul. 1995.

[21] C. Shauder and H. Mehta, "Vector analysis and control of advanced static VAR compensators," *Proc. Inst. Elect. Eng. C*, vol. 140, no. 4, pp. 299–306, Jul. 1993.

[22] P. Rao, M. L. Crow, and Z. Yang, "STATCOM control for power system voltage control application," *IEEE Trans. Power Delivery*, vol. 15, no. 4, pp. 1311–1317, Oct. 2000.

M. Tavakoli Bina (SM'07) received the B.Sc. and M.Sc. degrees from the University of Tehran, Tehran, Iran, in 1988 and 1991, respectively, and the Ph.D. degree from the University of Surrey, Guilford, U.K., in 2001, all in power electronics and power system utility applications.

From March 1992 to November 1997, he was with the K. N. Toosi University of Technology, Tehran, as a Lecturer working on power systems. In January 1998, he enrolled as a doctoral student in the Department of Electronics and Computer Engineering, University of Surrey. Since September 2001, he has been with the Faculty of Electrical and Computer Engineering, K. N. Toosi University of Technology (KNTU), Tehran. Currently, he is an Associate Professor at KNTU. His main research interests include power converters, modulation techniques, control and modeling of FACTS controllers, distribution systems, and power system control.

Ashoka K. S. Bhat (S'82–M'85–SM'87–F'98) received the B.Sc. degree in physics and math from Mysore University, India, in 1972, the B.E. degree (with distinction) in electrical technology and electronics and the M.E. degree (with distinction) in electrical engineering from the Indian Institute of Science, Bangalore, in 1975 and 1977, respectively, and the M.A.Sc. and Ph.D. degrees in electrical engineering from the University of Toronto, Toronto, ON, Canada, in 1982 and 1985, respectively.

From 1977 to 1981, he worked as a scientist in the Power Electronics Group, National Aeronautical Laboratory, Bangalore, India, and was responsible for the completion of a number of research and development projects. After working as a Postdoctoral Fellow for a short time, he joined the Department of Electrical Engineering, University of Victoria, Victoria, B.C., Canada, in 1985, where he is currently a Professor of Electrical Engineering and is engaged in teaching and conducting research in the area of power electronics. He was responsible for the development of the Electromechanical Energy Conversion and Power Electronics courses and laboratories in the Department of Electrical Engineering, University of Victoria.

Dr. Bhat is a Fellow of the Institution of Electronics and Telecommunication Engineers (India), and a registered Professional Engineer in the province of British Columbia, Canada.